What Is the Effect of Variational Optimization of the Transition State on α-Deuterium Secondary Kinetic Isotope Effects? A Prototype: $CD_3H + H \rightleftharpoons CD_3 + H_2$

Da-hong Lu, David Maurice, and Donald G. Truhlar*

Contribution from the Department of Chemistry and Supercomputer Institute, University of Minnesota, Minneapolis, Minnesota 55455-0431. *Received February 26, 1990*

Abstract: Variational Transition state theory calculations with semiclassical transmission coefficients have been carried out for a prototype case of α-deuterium secondary kinetic isotope effects (KIEs) in a reaction involving the transformation of an sp^3 carbon to sp^2, in particular for the reactions of CH_4 and CD_3H with H and D. We also study the KIE for the reverse direction and for the reactions of CH_4 and CD_3H with D. We find that the variational transition states lead to significantly different nontunneling KIEs than the conventional ones, e.g., 1.22 vs. 1.07, and the inclusion of multidimensional tunneling effects increases the discrepancy even more. The origins of these variational and tunneling effects are examined in detail in terms of structures, vibrational frequencies, and the curvature of the reaction path. The conclusions have wide implications for the validity of conventional treatments of kinetic isotope effects. We predict some particularly large secondary KIEs at low temperature, and these predictions can be tested by future experiments.

1. Introduction

The study of kinetic isotope effects (KIEs) on the rate constants of chemical reactions is an important tool for the elucidation of reaction mechanisms.[1-9] The KIE is the ratio of the rate constants for a pair of isotopically differentiated molecules; for deuterium KIEs, the ratio is taken as k_H/k_D, where k_H is the rate constant for the normal molecule and k_D is the rate constant for one in which one or more protiums are substituted by deuterium. A "normal" KIE is a ratio greater than unity, and an inverse isotope effect is a ratio less than unity. Deuterium KIEs for elementary steps can be classified as primary and secondary. Primary KIEs are associated with isotopic substitution in a bond that is broken or formed in the step. A secondary KIE is one due to isotopic substitution at spectator bonds. Secondary KIEs, especially α-deuterium isotope effects, have been widely studied for solvolysis processes.[3,8] The present study will investigate the effect on calculated secondary deuterium KIEs of variational optimization of the generalized transition state and of including tunneling by multidimensional semiclassical transmission coefficients.

"Transition state theory forms the basis of almost all of our discussions of isotope effects in chemical reactions."[8] In particular most discussions of KIEs have been based on conventional transition state theory (TST).[2-9] However, it is now well established that conventional transition state theory sometimes leads to large errors that can be considerably decreased by variational optimization of the transition state structure and the inclusion of multidimensional tunneling effects.[10-14] Variational transition state theory (VTST) has been applied to primary KIEs previously,[15-30] usually[16-30] with multidimensional transmission coefficients, but there has been only one previous application to secondary KIEs, namely to the degenerate gas-phase S_N2 reaction of Cl^- with CH_3Cl.[31]

The secondary deuterium KIE for the abstraction reaction of CH_3 with H_2 has previously been studied theoretically by Schatz

(1) Halevi, E. A. *Tetrahedron* **1957**, *1*, 174. Halevi, E. A. *Prog. Phys. Org. Chem.* **1963**, *1*, 109.
(2) Bigeleisen, J.; Wolfsberg, M. *Adv. Chem. Phys.* **1**, 15.
(3) Shiner, V. J. In *Isotope Effects in Chemical Reactions*; Collins, C. J., Bowman, N. S., Eds.; Van Nostrand Reinhold: New York, 1970; p 151. Sunko, D.-E.; Borcic, S. *Ibid.*, p 172.
(4) Scheppele, S. E. *Chem. Rev.* **1972**, *72*, 511.
(5) Shiner, V. J., Jr. *ACS Symp. Ser.* **1975**, *11*, 163.
(6) *Isotopes in Organic Chemistry*; Buncel, E., Lee, C. C., Eds.; Elsevier: Amsterdam; Vol. 1, 1975; Vol. 2, 1976.
(7) Hogg, J. L. In *Transition States of Biochemical Processes*; Gandour, R. D., Schowen, R. L., Eds.; Plenum: New York, 1978; p 201.
(8) Melander, L.; Saunders, W. H., Jr. *Reaction Rates of Isotopic Molecules*; Wiley: New York, 1980.
(9) Saunders, W. H., Jr. In *Investigation of Rates and Mechanisms of Reactions*; Bernasconi, C. F., Ed.; John Wiley & Sons: New York, 1986; Part 1, p 565.
(10) Truhlar, D. G.; Garrett, B. C. *Acc. Chem. Res.* **1980**, *13*, 440.
(11) Truhlar, D. G.; Hase, W. L.; Hynes, J. T. *J. Phys. Chem.* **1983**, *87*, 2664, 5523E.
(12) Truhlar, D. G.; Garrett, B. C. *Annu. Rev. Phys. Chem.* **1984**, *35*, 159.
(13) Truhlar, D. G.; Garrett, B. C. *J. Chim. Phys. Phys.-Chim. Biol.* **1987**, *84*, 365.
(14) Tucker, S. C.; Truhlar, D. G. In *New Theoretical Concepts for Understanding Organic Reactions*; Bertrán, J., Csizmadia, I. G., Eds.; Kluwer: Dordrecht, 1989; p 291.
(15) Garrett, B. C.; Truhlar, D. G. *J. Am. Chem. Soc.* **1979**, *101*, 4534. Garrett, B. C.; Truhlar, D. G. *J. Am. Chem. Soc.* **1980**, *102*, 2559.
(16) Garrett, B. C.; Truhlar, D. G. *J. Chem. Phys.* **1980**, *72*, 3460.
(17) Garrett, B. C.; Truhlar, D. G.; Grev, R. S.; Magnuson, A. W. *J. Phys. Chem.* **1980**, *84*, 1730.
(18) Garrett, B. C.; Truhlar, D. G.; Magnuson, A. W. *J. Chem. Phys.* **1981**, *74*, 1029; **1982**, *76*, 2321. Tucker, S. C.; Truhlar, D. G.; Garrett, B. C.; Isaacson, A. D. *J. Chem. Phys.* **1985**, *82*, 4102. Schwenke, D. W.; Tucker, S. C.; Steckler, R.; Brown, F. B.; Lynch, G. C.; Truhlar, D. G.; Garrett, B. C. *J. Chem. Phys.* **1989**, *90*, 3110.
(19) Isaacson, A. D.; Truhlar, D. G. *J. Chem. Phys.* **1982**, *76*, 1380.
(20) Truhlar, D. G.; Isaacson, A. D.; Skodje, R. T.; Garrett, B. C. *J. Phys. Chem.* **1982**, *86*, 2252. Bondi, D. K.; Clary, D. C.; Connor, J. N. L.; Garrett, B. C.; Truhlar, D. G. *J. Chem. Phys.* **1982**, *76*, 4986. Blais, N. C.; Truhlar, D. G.; Garrett, B. C. *J. Chem. Phys.* **1983**, *78*, 2363. Truhlar, D. G.; Grev, R. S.; Garrett, B. C. *J. Phys. Chem.* **1983**, *87*, 3415.
(21) Clary, D. C.; Garrett, B. C.; Truhlar, D. G. *J. Chem. Phys.* **1983**, *78*, 777.
(22) Garrett, B. C.; Truhlar, D. G.; Wagner, A. F.; Dunning, T. H., Jr., *J. Chem. Phys.* **1983**, *78*, 4400.
(23) Truhlar, D. G.; Garrett, B. C.; Blais, N. C. *J. Chem. Phys.* **1984**, *80*, 232. Brown, F. B.; Steckler, R.; Schwenke, D. W.; Truhlar, D. G.; Garrett, B. C. *J. Chem. Phys.* **1985**, *82*, 188. Steckler, R.; Truhlar, D. G.; Garrett, B. C. *J. Chem. Phys.* **1985**, *82*, 5499.
(24) Garrett, B. C.; Truhlar, D. G. *J. Chem. Phys.* **1984**, *81*, 309.
(25) Garrett, B. C.; Truhlar, D. G. *Int. J. Quantum Chem.* **1986**, *29*, 1463. Garrett, B. C.; Truhlar, D. G.; Bowman, J. M.; Wagner, A. F.; Robie, D.; Arepalli, S.; Presser, N.; Gordon, R. J. *J. Am. Chem. Soc.* **1986**, *108*, 3515. Garrett, B. C.; Truhlar, D. G. *Int. J. Quantum Chem.* **1987**, *31*, 81. Joseph, T.; Truhlar, D. G.; Garrett, B. C. *J. Chem. Phys.* **1988**, *88*, 6982.
(26) Garrett, B. C.; Truhlar, D. G.; Schatz, G. C. *J. Am. Chem. Soc.* **1986**, *108*, 2876.
(27) Joseph, T.; Steckler, R.; Truhlar, D. G. *J. Chem. Phys.* **1987**, *87*, 7036.
(28) Kreevoy, M. M.; Ostovič, D.; Truhlar, D. G.; Garrett, B. C. *J. Phys. Chem.* **1986**, *90*, 3766. Kreevoy, M. M.; Truhlar, D. G. In *Investigation of Rates and Mechanisms of Reactions*; Bernasconi, C. F., Ed.; Wiley: New York, 1986; Part I, p 13
(29) Garrett, B. C.; Steckler, R.; Truhlar, D. G. *Hyperfine Interactions* **1986**, *32*, 779.
(30) Garrett, B. C.; Joseph, T.; Truong, T. N.; Truhlar, D. G. *Chem. Phys.* **1989**, *136*, 271.
(31) Tucker, S. C.; Truhlar, D. G. *J. Am. Chem. Soc.* **1990**, *112*, 3338.

0002-7863/90/1512-6206$02.50/0

et al.[32] There are four key aspects of the present study that differentiate it from the previous work. First, we use VTST to locate the transition state dividing surface. Second, we include multidimensional tunneling effects in the transmission coefficient. Third, we base our results on a recent[27] semiglobal potential energy surface, whereas the previous work only used information about the surface in the quadratic regions around the reactant and the saddle point. Fourth, we consider both directions of reaction since they involve interesting differences.

The importance of variational effects on KIEs can be anticipated from the fact that in VTST there can be significant differences between the properties of the optimized transition states and the saddle point, which is the transition state in the conventional transition state theory calculations. Thus the energy, force constants, and bond distances of the optimized variational transition state for the isotopically substituted reaction may differ significantly from those for the unsubstituted reaction, whereas in conventional TST these quantities are independent of isotopic substitution. In addition, the effective potential for multidimensional tunneling calculations involves all of the vibrational frequencies, even those for "spectator" modes.[20,30,33-36]

Most of this article is concerned with the reactions

$$CH_4 + H \rightarrow CH_3 + H_2 \qquad \text{(reaction 1H)}$$

and

$$CD_3H + H \rightarrow CD_3 + H_2 \qquad \text{(reaction 1D)}$$

In section 4 though we briefly consider the reverse reactions and analogous reactions involving CD_3H and HD.

Although these reactions are of fundamental interest in their own right, our dynamical study of their secondary deuterium KIEs is also motivated by our goal of understanding the effects that may occur in more complicated processes, e.g., widely studied organic solvolyses and reactions of nucleophiles with esters.[37-40]

The contributions to the secondary deuterium KIEs will be carefully analyzed to determine the relative contributions of various modes to both the KIEs and the variational effects. This should improve our understanding of the quantitative reliability of interpretations of secondary KIEs in terms of the extent of rehybridization of the central carbon at the transition state. The central carbon atom in reaction 1H changes from tetrahedral sp^3 to plane trigonal sp^2. This type of conversion is found in many organic reactions and the interpretation of the extent of rehybridization is often used to classify the reaction mechanism,[1,4,5,8] although cases are known[41-47] where conclusions about transition state structure based on KIEs do *not* correlate well with other indices of transition state structure or with IR frequencies of reactants. The basic assumption underlying the correlation of k_H/k_D with transition state structure is that the out-of-plane bend mode of the sp^2 structure dominates the KIE. This mode of the sp^2 structure is expected to be looser than the mode it correlates with at the sp^3 structure, so k_H/k_D will be greater than 1 for an sp^3 reactant and an sp^2 transition state or product. Although exceptions are known, the previous conventional TST studies[32] on the deuterium KIE for the reactions studied here agree with the expectation based on the above considerations that secondary deuterium KIEs for the forward reactions are normal and the KIEs for the reverse reactions are inverse. This is also consistent with experiment.[48-50] We need, however, to understand the extent of the systematic error that is involved when one tries to relate the KIE to the structure of a transition state using conventional TST. Interpreting secondary deuterium KIEs with VTST should give more trustworthy pictures of the dynamical bottleneck for most reactions and should be more reliable for interpreting the reaction mechanisms.

For reaction 1H the rate constants have been measured[51] by using the flash photolysis-shock tube (FP-ST) technique, and reasonable agreement (~30%) with previous[27] VTST calculations was obtained.

According to the Born–Oppenheimer separation, the potential energy surface (PES) is independent of atomic masses. Thus for all isotopic combinations we use the same PES, in particular we use the semiglobal J1 analytic potential energy surface,[27] which is based in part on the ab initio calculations of Schatz, Wagner, Dunning, and Walch[32,52] and Sana et al.[53] This surface[27] has a classical endoergicity of 2.77 kcal/mol and classical barrier heights of 13.00 and 10.23 kcal/mol for the forward and reverse reactions, respectively. We will also present a few results for other surfaces to demonstrate that our qualitative conclusions are not overly dependent on unknown details.

In section 2 we present the method for computing the rate constants. The resulting secondary KIEs and their factorization into contributions from various degrees of freedom are presented in section 3. The reverse reaction and the reactions in which H_2 is substituted by HD are considered in section 4. Discussion and concluding remarks are given in section 5.

2. Method

VTST calculations were carried out by canonical variational theory (CVT).[10,36,54,55] First the minimum-energy path (MEP) of reaction is found by following the negative of the normalized gradient vector from the saddle point into both reactant and product valleys. All the calculations are performed in a mass-scaled Cartesian coordinate system[19,36] in which all atomic Cartesian coordinates are scaled by $(m_A/\mu)^{1/2}$ where m_A is the mass of the atom A and μ is a single mass to which all coordinates are scaled. In this study, the value of μ is taken as 1 amu. All distances, gradients, etc. are then computed and measured in this coordinate system. The negative gradient was followed by using an Euler single-step algorithm[36,56,57] with a fixed step size, e.g., 1.33×10^{-4} a_0 for reaction 1H. The signed distance from the saddle point along this path is called s. The hessian matrix is computed at larger intervals along the reaction path, e.g., 1.33×10^{-2} a_0 for reaction 1H, to obtain the generalized normal mode frequencies $\omega_m(s)$ and curvature coupling components[36,58] $B_{mF}(s)$, which were stored along with the geometries and

(32) Schatz, G. C.; Wagner, A. F.; Dunning, T. H., Jr. *J. Phys. Chem.* **1984**, *88*, 221.
(33) Skodje, R. T.; Truhlar, D. G.; Garrett, B. C. *J. Phys. Chem.* **1981**, *85*, 3019; *J. Chem. Phys.* **1982**, *77*, 5955.
(34) Garrett, B. C.; Truhlar, D. G. *J. Chem. Phys.* **1983**, *79*, 4931.
(35) Garrett, B. C.; Abusalbi, N.; Kouri, D. J.; Truhlar, D. G. *J. Chem. Phys.* **1985**, *83*, 2252.
(36) Truhlar, D. G.; Isaacson, A. D.; Garrett, B. C. In *The Theory of Chemical Reaction Dynamics*; Baer, M., Ed.; CRC Press: Boca Raton, FL, 1985; p 65.
(37) Streitwieser, A.; Jagow, R. H.; Fahey, R. C.; Suzuki, S. *J. Am. Chem. Soc.* **1958**, *80*, 2326.
(38) Llewellyn, J. A.; Robertson, R. E.; Scott, J. M. W. *Can. J. Chem.* **1960**, *38*, 222.
(39) Bilkadi, Z.; de Lorimier, R.; Kirsch, J. F. *J. Am. Chem. Soc.* **1975**, *97*, 4317.
(40) do Amaral, L.; Bastos, M. P.; Bull, H. G.; Ortiz, J. J.; Cordes, E. H. *J. Am. Chem. Soc.* **1979**, *101*, 169.
(41) Pohl, E. R.; Hupe, D. J. *J. Am. Chem. Soc.* **1980**, *102*, 2763.
(42) Kurz, L. C.; Frieden, C. *J. Am. Chem. Soc.* **1980**, *102*, 4198.
(43) Knier, B. L.; Jencks, W. P. *J. Am. Chem. Soc.* **1980**, *102*, 6789.
(44) Ostovič, D.; Roberts, R. M. G.; Kreevoy, M. M. *J. Am. Chem. Soc.* **1983**, *105*, 7629. For subsequent work on these reactions see: reference 28. Kreevoy, M. M.; Kotchevar, A. T. *J. Am. Chem. Soc.* **1990**, *112*, 3579. Kreevoy, M. M.; Lee, I.-S. H. *Z. Naturforsch.* **1989**, *44a*, 418.
(45) Huskey, W. P.; Schowen, R. L. *J. Am. Chem. Soc.* **1983**, *105*, 5704.
(46) Saunders, W. H., Jr. *J. Am. Chem. Soc.* **1984**, *106*, 2223; **1985**, *107*, 164. Amin, M.; Price, R. C.; Saunders, W. H., Jr. *J. Am. Chem. Soc.* **1990**, *112*, 4467.
(47) Cha, Y.; Murray, C. J.; Klinman, J. P. *Science* **1989**, *243*, 1325. Grant, K. L.; Klinman, J. P. *Biochemistry* **1989**, *28*, 6597.
(48) Shapiro, J. S.; Weston, R. E. *J. Phys. Chem.* **1972**, *76*, 1669.
(49) Majury, T. G.; Steacie, E. W. R. *Can. J. Chem.* **1952**, *30*, 800.
(50) Kerr, J. A.; Parsonage, M. J. *Evaluated Kinetic Data on Gas Phase Hydrogen Transfer Reactions of Methyl Radicals*; Butterworths: London, 1976.
(51) Robinowitz, M. J.; Sutherland, J. W.; Patterson, P. M.; Klemm, R. B. *J. Phys. Chem.* In press.
(52) Walch, S. P. *J. Chem. Phys.* **1980**, *72*, 4932. Schatz, G. C.; Walch, S. P.; Wagner, A. F. *J. Chem. Phys.* **1980**, *73*, 4536.
(53) Sana, M.; LeRoy, G.; Villaveces, J. L. *Theor. Chim. Acta* **1984**, *65*, 109.
(54) Eliason, M. A.; Hirschfelder, J. O. *J. Chem. Phys.* **1959**, *30*, 1426.
(55) Garrett, B. C.; Truhlar, D. G. *J. Chem. Phys.* **1979**, *70*, 1593; *J. Phys. Chem.* **1979**, *83*, 1052, 1079; **1983**, *87*, 4553E.
(56) Isaacson, A. D.; Truhlar, D. G.; Rai, S. N.; Steckler, R.; Hancock, G. C.; Garrett, B. C.; Redmon, M. J. *Comput. Phys. Commun.* **1987**, *47*, 91.
(57) Garrett, B. C.; Redmon, M. J.; Steckler, R.; Truhlar, D. G.; Baldridge, K. K.; Bartol, D.; Schmidt, M. W.; Gordon, M. S. *J. Phys. Chem.* **1988**, *92*, 1476.

classical potential, $V_{MEP}(s)$, along the path.

In the CVT calculations, the generalized transition state is optimized canonically by finding the maximum of the generalized free energy of activation with respect to s using interpolation and the stored quantities just mentioned. Given the location, $s_*^{CVT}(T)$, of the generalized transition state, the canonical variational theory rate constants, k^{CVT}, which do not include tunneling, are computed from the energies and partition functions of the reactants and variational transition states.

Including a ground-state (G) transmission coefficient $\kappa^{CVT/G}(T)$ to account for quantum mechanical tunneling yields[10,16,17]

$$k^{CVT/G} = \kappa^{CVT/G}(T)k^{CVT}(T) \quad (1)$$

Two types of multidimensional semiclassical tunneling calculations were performed, with each accounting for curvature coupling of the reaction path to the generalized normal modes in a different way. In particular we employed the small-curvature semiclassical adiabatic ground-state (SCSAG) tunneling approximation[33,36] and the large-curvature semiclassical ground-state tunneling approximation, version 3 (LCG3).[30,35,36] For all reactions included in this study (see sections 3 and 4), the angle[36] between the reactant and product valleys in mass-scaled coordinates is between 37.4 and 46.8°, which yields "intermediate" reaction-path curvature. For such cases, as well as for large-curvature systems, the tunneling is usually underestimated by both SCSAG and LCG3 calculations.[34] For such intermediate-curvature cases, whichever of these methods yields a larger transmission coefficient is therefore assumed to be more reliable. Performing both an SCSAG and an LCG3 calculation and accepting the larger answer may be thought of as a poor man's version of the least-action ground-state (LAG) model,[34] in which the reaction-path-curvature effects on tunneling are treated with more fine tuning. Thus we will set κ^G equal to whichever of these transmission coefficients is larger.

All calculations were performed with a new version of the polyatomic variational transition state theory program POLYRATE. (The original version of POLYRATE is available in the Computer Physics Communications International Program Library.[56]) Vibrations were treated as quantum mechanical harmonic oscillators and rotations as classical rigid rotators.

For comparison, we also evaluated conventional transition state theory (TST) rate constants, k^*, which result from locating the transition state dividing surface at the saddle point of the potential energy surface. The conventional TST rate constants were also corrected to second order in $\hbar$ with the popular[2,8,32] semiclassical Wigner[59] correction κ^W, which yields

$$k^{*/W} = \kappa^W k^* \quad (2a)$$

where

$$\kappa^W = 1 + \frac{(u^*)^2}{24} \quad (2b)$$

where $u^* = hc\nu^*/\tilde{k}T$, where h is Planck's constant, c is the speed of light, ν^* is imaginary frequency in wavenumbers, $\tilde{k}$ is Boltzmenn's constant, and T is temperature. Since κ^W depends only on the imaginary frequency along the reaction coordinate at the saddle point, it is a one-dimensional transmission coefficient. Another popular tunneling correction for conventional TST is based on tunneling through a one-dimensional infinite parabolic (IP) barrier with the same imaginary frequency as the saddle point. This yields[8,60]

$$k^{*/IP} = \kappa^{IP} k^* \quad (2c)$$

where

$$\kappa^{IP} = \frac{(u^*)/2}{\sin(u^*/2)} \quad (2d)$$

Both $k^{CVT}(T)$ and $k^*(T)$ contain a symmetry number σ whose effect is dynamically trivial. It makes the interpretation more clear to factor this out so we write[8]

$$\frac{k_H}{k_D} = \frac{\sigma_H}{\sigma_D}\eta \quad (3)$$

This defines the per-site secondary deuterium kinetic isotope effect η. As an example we note that $\eta = (1/4)k_H/k_D$ for the $CH_4/CD_3H + H \rightarrow CH_3/CD_3 + H_2$ case. Values of η obtained by different versions of TST will be labeled by superscripts, i.e., η^{CVT}, $\eta^{CVT/G}$, η^*, $\eta^{*/W}$, etc.

It will be informative to factor η into contributions from the two factors of eqs 1 and 2, e.g.,

$$\eta^{CVT/G} = \eta_{tun}^{CVT}\eta^{CVT} \quad (4)$$

where

$$\eta_{tun}^{CVT} = \kappa_H^{CVT/G}/\kappa_D^{CVT/G} \quad (5)$$

By using the basic expression[36] of a generalized transition state rate constant as $\tilde{k}T/h$ times a ratio of partition functions times a Boltzmann factor, the per-site KIEs calculated with unit transmission coefficients (η^{CVT} and η^*) are further factored, e.g.,

$$\eta^{CVT} = \frac{Q_H^{GT}[T,s_{*,H}^{CVT}(T)]\Phi_D^R(T)\exp\{-V_{MEP}[s_{*,H}^{CVT}(T)]/\tilde{k}T\}}{Q_D^{GT}[T,s_{*,D}^{CVT}(T)]\Phi_H^R(T)\exp\{-V_{MEP}[s_{*,D}^{CVT}(T)]/\tilde{k}T\}} \quad (6)$$

where $Q^{GT}[T,s_*^{CVT}(T)]$ is the partition function of the variational transition state, $V_{MEP}[s_*^{CVT}(T)]$ is the classical potential at the variational transition state at $s_*^{CVT}(T)$, and $\Phi^R(T)$ is the reactant partition function per unit volume. For η^*, the function Q^{GT} in eq 6 is replaced by Q^*, which is the partition function at the saddle point ($s = 0$), and V_{MEP} is also evaluated at the saddle point.

By assuming negligible coupling between electronic, vibrational, and rotational energies and also assuming that the electronic partition functions cancel completely in the KIEs, the η^{CVT} ratios can be factored as follows:

$$\eta^{CVT} = \eta_{trans}\eta_{rot}^{CVT}\eta_{vib}^{CVT}\eta_{pot}^{CVT} \quad (7)$$

where the four factors represent the contributions from the translational, rotational, and vibrational partition functions and the Boltzmann factor associated with the potential V_{MEP}. The factor η_{trans} differs from unity because the reduced mass changes upon isotopic substitution. The factor η_{rot}^{CVT} differs from unity because the moments of inertia change—both because of the change in mass and also because the bond distances and bond angles change when the variational transition state structure is re-optimized for each isotopic reaction. The factor η_{vib}^{CVT} differs from unity because the vibrational partition functions change—both directly as a result of the change in mass and also because of the change in force constants which results from re-optimization of the variational transition state structure upon isotopic substitution. The factor η_{pot}^{CVT} differs from unit entirely because of the structure re-optimization.

The conventional transition state theory per-site KIE, η^*, can also be factored as in (6). There is no change in η_{trans}, but η_{rot}^* and η_{vib}^* differ from unity only because of the mass change (they are evaluated at the same transition state structure, in particular the saddle point, for both isotopic reactions in the ratio), and η_{pot}^* is unity.

More specifically,

$$\eta_{trans} = \Phi_{rel,D}^R/\Phi_{rel,H}^R \quad (8)$$

where $\Phi_{rel,X}^R$ is the relative translational partition function per unit volume for the reactants in reaction 1X;

$$\eta_{rot}^{CVT} = \frac{Q_{rot,H}^{GT}Q_{rot,D}^R}{Q_{rot,D}^{GT}Q_{rot,H}^R} \quad (9)$$

where $Q_{rot,X}^{GT}$ is the generalized transition state rotational partition function, and $Q_{rot,X}^R$ is the reactant rotational partition function;

$$\eta_{vib}^{CVT} = \frac{Q_{vib,H}^{GT}Q_{vib,D}^R}{Q_{vib,D}^{GT}Q_{vib,H}^R} \quad (10)$$

where $Q_{vib,X}^{GT}$ and $Q_{vib,X}^R$ are vibrational partition functions; and

$$\eta_{pot}^{CVT} = \exp\{-[V_{MEP}(s_{*,H}^{GT}) - V_{MEP}(s_{*,D}^{GT})]/\tilde{k}T\} \quad (11)$$

where $s_{*,X}$ is the generalized transition state location. In conventional transition state theory calculations, all the properties of generalized transition states are evaluated at the saddle point ($s = 0$). Notice that the reactant contributions to (9) and (10) are entirely due to CH_4 or CD_3H; all atomic properties cancel in the secondary deuterium KIEs.

In order to analyze the relative importance of different normal mode motions, the vibrational contribution of eq 10 is further factored according to the correlations of vibrational degrees of freedom between the generalized transition states and the corresponding reactants. These correlations are given in Table I. (The columns headed $CH_3 + H_2$ and $CD_3 + H_2$ are not involved in this correlation, but they are needed for the reverse reaction discussed in section 4.) In the subscripts (i.e., ν_1, ν_2, ...), the vibrational frequencies of CH_4, H_3C–H–H, CD_3H, and

(58) Miller, W. H.; Handy, N. C.; Adams, J. E. *J. Chem. Phys.* **1980**, *72*, 99.

(59) Wigner, E. P. *Z. Phys. Chem.* **1932**, *B19*, 203.

(60) Bell, R. P. *Trans. Faraday Soc.* **1959**, *55*, 1. Quickert, K. A.; LeRoy, D. J. *J. Chem. Phys.* **1970**, *52*, 856. Bell, R. P. *The Tunnel Effect in Chemistry*; Chapman & Hall: London, 1980; pp 60–63. The infinite parabolic formula is discussed further in: Skodje, R. T.; Truhlar, D. G. *J. Phys. Chem.* **1981**, *85*, 624.

Table I. Correlations of Calculated Harmonic Frequencies for CH_4, H_3C–H–H, and $CH_3 + H_2$ and for CD_3H, D_3C–H–H, and $CD_3 + H_2$[a]

m	g_m	CH_4	H_3C–H–H	$CH_3 + H_2$	CD_3H	D_3C–H–H	$CD_3 + H_2$
1	1	$\nu_1(a_1) = 2876$	$\nu_1(a_1) = 3103$	$\nu_1(a_1') = 2986$	$\nu_2(a_1) = 2085$	$\nu_1(a_1) = 2228$	$\nu_1(a_1') = 2111$
2	1	$\nu_3(t_1) = 3027$	$\nu_2(a_1) = 1720$	$\nu_{H_2} = 4405$	$\nu_1(a_1) = 3005$	$\nu_2(a_1) = 1713$	$\nu_{H_2} = 4405$
3	1	$\nu_4(t_2) = 1337$	$\nu_3(a_1) = 1131$	$\nu_2(a_1'') = 580$	$\nu_3(a_1) = 1022$	$\nu_3(a_1) = 864$	$\nu_2(a_1'') = 449$
4	2	$\nu_3(t_1) = 3027$	$\nu_4(e) = 3123$	$\nu_3(e) = 3173$	$\nu_4(e) = 2268$	$\nu_4(e) = 2329$	$\nu_3(e) = 2373$
5	2	$\nu_2(e) = 1505$	$\nu_5(e) = 1379$	$\nu_4(e) = 1383$	$\nu_5(e) = 1281$	$\nu_5(e) = 1156$	$\nu_4(e) = 1013$
6	2	$\nu_4(t_2) = 1337$	$\nu_6(e) = 1212$		$\nu_6(e) = 1033$	$\nu_6(e) = 997$	
7	2		$\nu_7(e) = 592$			$\nu_7(e) = 496$	

[a] Frequencies are in units of cm^{-1}; the symmetry labels are in parentheses.

D_3C–H–H are each numbered independently in the conventional way. In addition, a global mode numbering scheme (m = 1, 2, ..., 7) is indicated in the first column of the table. The correlation of the normal modes of CH_4 to those of H_3C–H–H will be discussed to illustrate the correlations. At the saddle point or a generalized transition state, the eleven bound generalized normal modes consist of three nondegenerate modes and four doubly degenerate modes. Mode ν_1 of H_3C–H–H with a_1 symmetry correlates to the nondegenerate CH stretch ν_1 in CH_4 so no renumbering is required for these modes. However, mode ν_2 of H_3C–H–H, again with a_1 symmetry, is correlated to one component of the triply degenerate CH stretch, ν_3, of CH_4 so the latter's partition function is labeled $Q^R_{vib,2}$ rather than $Q^R_{vib,3}$. The umbrella mode ν_3 of H_3C–H–H with a_1 symmetry is correlated to one component of the triply degenerate mode $\nu_4(t_2)$ in CH_4 so this component's vibrational partition function is labeled $Q^R_{vib,3}$. Mode ν_4 of H_3C–H–H with e symmetry is correlated to two components of the triply degenerate CH stretch, $\nu_3(t_1)$, in CH_4; the partition functions of these modes are indexed m = 4 all along the reaction path and at reactants. Mode $\nu_5(e)$ of the transition state correlates to the doubly degenerate bend, $\nu_2(e)$, in CH_4; the partition function for a component of this reactant mode is therefore called $Q^R_{vib,5}$. Mode $\nu_6(e)$ of H_3C–H–H is correlated to two components of the triply degenerate H–C–H bending motion, $\nu_4(t_2)$, in CH_4 so that the vibrational partition functions of these components are referred to as $Q^R_{vib,6}$. Mode $\nu_7(e)$ of H_3C–H–H does not correlate to a bound motion of CH_4.

The overall vibrational contribution to the secondary KIEs can then be factored as

$$\eta^{CVT}_{vib} = \prod_{m=1}^{7} (\eta^{GT}_{vib,m} \cdot \eta^{R}_{vib,m})^{g_m} = \prod_{m=1}^{7} \eta^{CVT}_{vib,m} \quad (12)$$

where g_m is the global degeneracy (1 or 2) of the mode m,

$$\eta^{GT}_{vib,m} = \frac{Q^{GT}_{vib,m,H}}{Q^{GT}_{vib,m,D}} \quad (13)$$

and

$$\eta^{R}_{vib,m} = \frac{Q^{R}_{vib,m,D}}{Q^{R}_{vib,m,H}} \quad (14)$$

and $\eta^R_{vib,7} = 1$. Similar factorizations are performed in the analysis of the results from the conventional TST calculations except that $Q^{GT}_{vib,m}$, $\eta^{GT}_{vib,m}$, and $\eta^{CVT}_{vib,m}$ are replaced by $Q^{\ddagger}_{vib,m}$, $\eta^{TS}_{vib,m}$, and $\eta^{\ddagger}_{vib,m}$, respectively, which can be evaluated from the properties of the saddle points for the corresponding reactions.

In order to illustrate the importance of including the tunneling effect, the Arrhenius parameters $A_{H(D)}$ and $E_{a,H(D)}$ are obtained by fitting the rate constants at pairs of temperatures. In studies of primary KIEs, the ratios of pre-exponential factors (A_H/A_D) and the differences of activation energies ($E_{a,H} - E_{a,D}$) have been used[61] as indications of the importance of tunneling for "normal" deuterium KIEs. The difference between $\eta^{CVT/G}$ and η^{CVT} and the differences between the values of $E_{a,H} - E_{a,D}$ or A_H/A_D obtained from $\eta^{CVT/G}$ and η^{CVT} may also be used to provide a measure of the importance of including tunneling in secondary KIEs.

3. Results: Forward Reaction

1. Net KIE. The transmission coefficients for reactions 1H and 1D are given in Table II for the two semiclassical methods employed as well as for the Wigner and infinite parabolic methods. We see that both multidimensional semiclassical tunneling methods predict much larger tunneling contributions than the Wigner method as well as a much greater isotopic sensitivity. The treatment based on an infinite parabola yields more tunneling, but again there is very little isotopic sensitivity. As discussed in section 2 we accept the larger of the SCSAG and LCG3 transmission coefficients as most reliable, and hence in the remainder of the discussion we shall employ the SCSAG transmission coefficients for both reactions 1H and 1D.

Table II. Transmission Coefficients for Reactions 1H and 1D as Functions of T

reactant	κ	200 K	250 K	300 K	400 K	500 K	600 K
CH_4	W	3.11	2.35	1.94	1.53	1.34	1.23
	IP	*a*	9.74	3.40	1.82	1.44	1.28
	SCSAG	69.2	12.3	5.27	2.44	1.75	1.47
	LCG3	59.0	9.95	4.11	1.96	1.48	1.30
CD_3H	W	3.07	2.33	1.92	1.52	1.33	1.23
	IP	*a*	9.01	3.31	1.80	1.43	1.27
	SCSAG	45.4	9.60	4.52	2.27	1.67	1.43
	LCG3	24.4	5.90	3.00	1.71	1.38	1.24

[a] The infinite parabolic formula is not applicable at 200 K since $u^{\ddagger}$ exceeds 2π; in particular it equals 7.11 for CH_4 + H and 7.06 for CD_3H + H.

Table III. Per-Site Secondary Deuterium KIEs for CH_4/CD_3H + H → CH_3/CD_3 + H_2

T, K	$\nu^{\ddagger}$	$\eta^{\ddagger/W}$	$\eta^{\ddagger/IP}$	η^{CVT}	$\eta^{CVT/G}$
200	1.07	1.08	*a*	1.30	2.04
250	1.08	1.09	1.16	1.27	1.63
300	1.07	1.08	1.10	1.22	1.42
372	1.06	1.06	1.07	1.12	1.27
400	1.05	1.05	1.06	1.13	1.23
500	1.03	1.03	1.04	1.08	1.14
600	1.02	1.02	1.02	1.05	1.10
1000	1.00	1.00	1.00	1.00	1.04
1500	1.00	1.00	1.00	1.00	1.03

[a] See footnote *a* in Table II.

Table IV. Kinetic Isotope Effects on Per-Site Arrhenius Parameters for Reactions 1H and 1D at 300–372 K

	A_H/A_D	$E_{a,D} - E_{a,H}$, kcal/mol
‡	0.99	0.046
‡/W	0.99	0.052
‡/IP	0.95	0.087
CVT	0.92	0.17
CVT/G	0.79	0.35

The per-site secondary deuterium KIEs calculated by CVT and conventional TST with the SCSAG transmission coefficient are listed in Table III for the CH_4 + H reaction. As anticipated in the Introduction, all these KIEs are greater than unity. The KIEs calculated by conventional TST, by CVT, and by CVT with the SCSAG transmission coefficient are illustrated in Figure 1. The tunneling correction raises the KIE by a factor [η^{CVT}_{tun}, see eq 5] equal to 1.52, 1.28, 1.17, and 1.08 at 200, 250, 300, and 400 K, respectively. These factors are much larger than typical experimental uncertainties and indicate that tunneling must be considered for quantitative interpretations of the KIE, *even though the Wigner approximation would indicate only a 1% effect.* The Wigner method predicts a small effect (small difference between $\eta^{\ddagger}$ and $\eta^{\ddagger/W}$) because there is hardly any change in the imaginary frequency at the saddle point upon substituting CD_3 for CH_3. In particular the imaginary frequency changes from 989i cm^{-1} for H_3C–H–H to 981i cm^{-1} for D_3C–H–H. The use of κ^W in refs 8 and 32 would thus appear to be a serious possible source of error

(61) See, e.g.: Kaldor, S. B.; Saunders, W. H., Jr. *J. Chem. Phys.* **1978**, *68*, 2509.

Table V. The Geometries and Properties of Transition States, $H_3C{-}{-}H_a{-}{-}H_b$ or $D_3C{-}{-}H_a{-}{-}H_b$, for Reactions 1H and 1D[a]

	s, a_0	V_{MEP}	V_a^G	R_{CH_a}	R_{CH} or R_{CD}[b]	$R_{H_aH_b}$	angle H-C-H or D-C-D	angle H-C--H_a or D-C--H_a	generalized-transition-state frequencies,[c] cm^{-1}
$H_3C{-}{-}H_a{-}{-}H_b$									
conv. TS[d]	0	13.00	39.54	2.544	2.072	1.701	112.24	106.57	3102, 1719, 1130, 3123 (2), 1378 (2), 1211 (2), 591 (2)
CVT, 300 K	0.11	12.91	39.64	2.650	2.071	1.619	112.72	105.98	3082, 2195, 1074, 3135 (2), 1353 (2), 1117 (2), 571 (2)
$D_3C{-}{-}H_a{-}{-}H_b$									
conv. TS[d]	0	13.00	34.10	2.544	2.072	1.701	112.24	106.57	2227, 1713, 863, 2328 (2), 1155 (2), 997 (2), 495 (2)
CVT, 300 K	0.13	12.86	34.31	2.677	2.070	1.603	112.81	105.92	2347, 2184, 816, 2339 (2), 1044 (2), 978 (2), 465 (2)

[a] The classical potential V_{MEP} and the vibrationally adiabatic ground-state potential V_a^G are in units of kcal/mol; the bond distances R_{XY} are in units of a_0, and the bond angles are in deg. [b] Spectator bond lengths. [c] The number in parentheses is the degeneracy of the mode. [d] Conventional transition state.

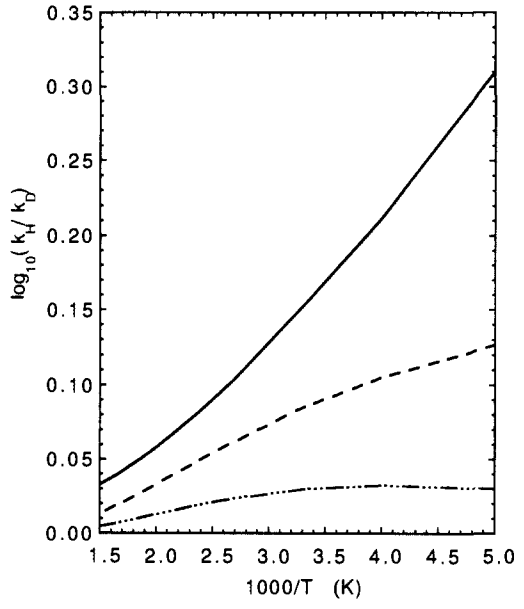

Figure 1. Logarithm of the per-site secondary deuterium KIE for reactions 1H and 1D vs $1000/T$: (—) results from the CVT calculation with tunneling; (---) results from the CVT calculation without tunneling; and (--) results from the conventional TST calculation without tunneling.

in that work. The infinite parabolic formula suffers from similar deficiencies. Tunneling formulas based only on the imaginary frequency at the barrier are qualitatively incorrect.

Table IV shows the effect of deuterium substitution on the Arrhenius parameters. The effect on the pre-exponential factor A is striking in that VTST predicts a significantly larger effect than does conventional TST, and the effect is amplified by tunneling. VTST also shows a much bigger effect on the activation energy, again amplified by tunneling.

The variational effect on the secondary deuterium KIEs, i.e., the effect of where the dividing surface is located, can be ascertained by comparison of the ratios of the rate constants calculated by variational and conventional TST in the absence of tunneling. Table III and Figure 1 show that the effect is large, about 15% at 300 K. The geometries and properties of transition states calculated by conventional TST and CVT for reactions 1H and 1D are listed in Table V. We see that the variational transition states are slightly more than 0.1 a_0 closer to products than the saddle point is. This places them where the potential energy is about 0.1 kcal/mol lower, the bond angles differ by about 0.6°, and vibrational frequencies differ by 11–476 cm^{-1} from their values at the saddle point. The direction of the change in transition state location is the same as predicted earlier by a 3-body RMBEBO model.

2. Factor Analysis. According to eqs 7–11 the secondary deuterium KIEs calculated without tunneling corrections can be factored in terms of the contributions of the translational, rotational, and vibrational motions and the potential along the MEP. The factored contributions are given in Table VI. For the conventional TST calculations, the classical potential differences between the transition state and the reactions do not contribute

Table VI. The Contributions of Various Types of Motion to η^* and η^{CVT} for the Reactions $CH_4/CD_3H + H \rightarrow CH_3/CD_3 + H_2$

T, K	η_{trans}	η^*_{rot}	η^*_{vib}	η^{CVT}_{rot}	η^{CVT}_{vib}	η^{CVT}_{pot}
200	1.01	1.27	0.83	1.27	1.17	0.86
250	1.01	1.27	0.84	1.27	1.11	0.90
300	1.01	1.27	0.83	1.27	1.03	0.92
372	1.01	1.27	0.82	1.27	0.93	0.94
400	1.01	1.27	0.81	1.27	0.92	0.95
500	1.01	1.27	0.80	1.27	0.87	0.97
600	1.01	1.27	0.79	1.27	0.83	0.98
1000	1.01	1.27	0.78	1.27	0.78	1.00
1500	1.01	1.27	0.78	1.27	0.78	1.00

to the KIEs because of the invariance of the potential energy surface and transition state location for isotopic molecules, i.e., $\eta^*_{pot} = 1$. In CVT calculations, the potential contribution to the secondary deuterium KIE, η^{CVT}_{pot}, results from the different classical potentials of the generalized transition states of the deuterated and undeuterated reactions. For reactions 1H and 1D, this makes an inverse contribution of about 10% at and below room temperature. Table VI shows that this contribution becomes less important as the temperature increases.

The contribution of translational motion of the reactants is the same in both conventional TST and CVT calculations and is given by

$$\eta_{trans} = \left(\frac{\mu_{CD_3H+H}}{\mu_{CH_4+H}}\right)^{3/2} \qquad (15)$$

It clearly gives a small normal contribution to the second deuterium KIEs.

In conventional TST, the rotational contribution to the secondary deuterium KIEs results from the balance of two ratios of square roots of products of principal moments of inertia. One ratio refers to CD_3H and CH_4 and gives a normal contribution. The second ratio refers to the products of the moments of inertia for the $H_3C{-}H{-}H$ and $D_3C{-}H{-}H$ saddle points and gives an inverse effect. The first ratio, which is about 2.27, gives the dominant contribution so that the total rotational effect is normal, as seen in Table VI. Since, as we saw in Table V, the geometrical shift of the variational transition state from the saddle points is small and similar for the two isotopic reactions, η^{CVT}_{rot} is similar to η^*_{rot}; in fact, it is the same to three significant figures. This factor would of course be smaller for higher molecular weight reactants.

There is a large variational effect on the vibrational contribution to the KIEs for the isotopic pair of reactions 1H and 1D at low temperatures, which can be observed from the differences between η^*_{vib} and η^{CVT}_{vib} listed in Table VI. At room temperature and below the two theories even predict different directions for the effect. In this temperature range, the vibrations provide an inverse contribution to the secondary deuterium KIE in conventional TST (i.e., $\eta^*_{vib} < 1$). Since, for temperatures above room temperature, both conventional and variational TST give an inverse vibrational contribution to the KIE, it would be wrong to interpret this normal KIE as resulting primarily from vibrations, which is the "textbook" approach.

Further factorization of η^*_{vib} and η^{CVT}_{vib} was performed by using the correlations of Table I and eqs 12–14. For reactions 1H and

Table VII. The Contributions of Various Modes or Degenerate Pairs of Modes to η^{*}_{vib} and η^{CVT}_{vib} for $CH_4/CD_3H + H \rightarrow CH_3/CD_3 + H_2$

	$\eta_{vib,1}$		$\eta_{vib,2}$		$\eta_{vib,3}$		$\eta_{vib,4}$		$\eta_{vib,5}$		$\eta_{vib,6}$		$\eta_{vib,7}$	
T, K	‡	CVT	‡	CVT	‡	CVT	‡	CVT	‡	CVT	‡	CVT	‡	CVT
200	0.74	1.46	1.11	0.96	1.22	1.26	0.85	0.84	1.01	0.50	2.00	3.60	0.49	0.44
250	0.79	1.27	1.08	1.01	1.17	1.20	0.88	0.88	1.00	0.59	1.74	2.75	0.55	0.50
300	0.82	1.14	1.07	1.06	1.14	1.15	0.90	0.89	1.00	0.66	1.59	2.29	0.59	0.55
372	0.85	1.02	1.06	1.11	1.10	1.12	0.92	0.91	1.00	0.73	1.46	1.90	0.62	0.58
400	0.86	0.99	1.05	1.14	1.09	1.10	0.92	0.92	1.00	0.75	1.42	1.81	0.63	0.60
500	0.89	0.93	1.04	1.16	1.07	1.07	0.94	0.94	0.99	0.82	1.33	1.57	0.66	0.63
600	0.91	0.92	1.03	1.14	1.05	1.05	0.95	0.95	0.99	0.86	1.28	1.43	0.67	0.65
1000	0.95	0.95	1.02	1.06	1.02	1.02	0.97	0.97	0.98	0.94	1.20	1.22	0.69	0.68
1500	0.97	0.97	1.02	1.04	1.01	1.01	0.99	0.98	0.98	0.96	1.17	1.17	0.70	0.70

1D, the seven contributions from the different vibrational motions to the secondary deuterium KIEs for reactions 1H and 1D are listed in Table VII, and the generalized normal mode frequencies along the reaction paths over the range from $s = -0.10\ a_0$ to $s = 0.20\ a_0$ for reactions 1H and 1D are plotted in Figure 2, a and b.

There are three major inverse contributions to the KIE, and these come from vibrations 4, 5, and 7, each of which is doubly degenerate. Taken together these three vibrations are responsible for the net inverse vibrational contribution, $\eta^{CVT}_{vib} < 1$. The lowest frequency mode ν_7 of the transition states, which does not correlate to a bound vibrational motion of CH_4 or CD_3H and hence may be called a transition mode, gives the most important inverse contribution. The $m = 5$ vibration, which correlates to an H–C–H bending motion in CH_4, also gives a substantial inverse contribution at low temprature, and the $m = 4$ vibration, which evolves asymptotically into an asymmetric C–H stretch, gives the third most significant inverse contribution at low temperature, as seen in Table VII.

From the results presented in Table VII, it is clear that the overall vibrational contribution to the secondary deuterium KIE is the result of a complicated balance from several competing effects, some normal and some inverse, with the net result much smaller than the components. We may compare the situation to that assumed in the classic paper of Streitwieser et al.[37] on reactions of sp^3 substrates proceeding through sp^2 transition states (this paper is still generally accepted[8] as providing the correct qualitative explanation of α-deuterium KIEs in such reactions). Streitwieser et al.[37] assumed that the out-of-plane (umbrella) mode (here $m = 3$) dominates the α-deuterium secondary KIE because other frequencies were not expected to change as much in passing from the reactants to the transition state. Table VII shows, however, that the present more detailed calculations provide a much more complicated picture.

Another important aspect of Table VII is that it shows the extent to which variational effects change the contributions from the various vibrational motions. This can be observed by comparison of $\eta^{CVT}_{vib,m}$ to $\eta^{*}_{vib,m}$. Since $s^{CVT}_{*}(300\ K) = 0.11\ a_0$ for reaction 1H, the major variational effect on the generalized normal mode frequencies would ordinarily be expected to arise principally from the mode or modes that vary most rapidly in the range $0 \le s \le 0.11\ a_0$. Parts a and b of Figure 2 show that mode 2 has the most rapid variation in this range for both reactions 1H and 1D. For reaction 1H this mode is correlated to one component of the triply degenerate C–H stretch of CH_4. However, the variational effect on the secondary KIE is determined by ratios involving the generalized normal modes for both the unsubstituted and substituted reaction, and it must be understood in terms of the net balance of the effects. As Figure 2a so clearly shows, the frequency changes are almost identical for reactions 1H and 1D for mode 2 so the variational effect on the KIE is not very large because of cancellation. Instead other modes involving less cancellation contribute more to the difference between η^{*} and η^{CVT}. These modes are considered next.

At 300 K, there is a significant difference between $\eta^{*}_{vib,5}$ and $\eta^{CVT}_{vib,5}$; in particular mode 5 provides an inverse contribution in the variational calculation ($\eta^{CVT}_{vib,5} < 1$) but a negligible one in the conventional TST calculation ($\eta^{*}_{vib,5} \cong 1$). Similarly the CVT calculation yields a normal contribution of 1.14 from the ν_1 vibration at 300 K, whereas conventional TST yields an inverse contribution of 0.82. These significant differences show that there

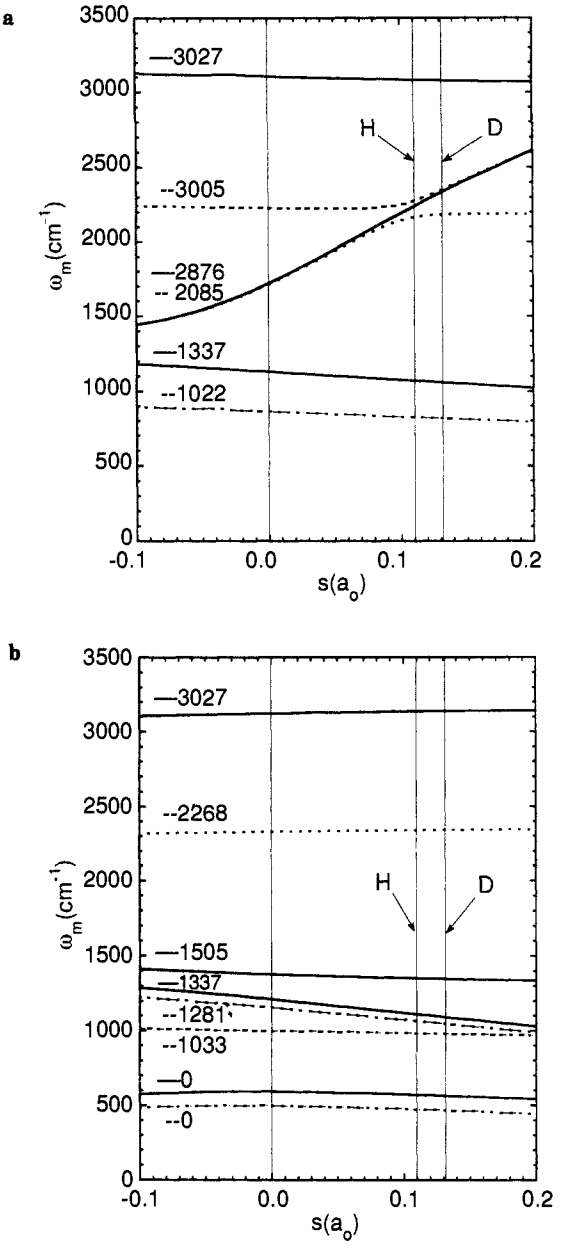

Figure 2. (a) Frequencies of the generalized normal modes with a symmetry (modes 1, 2, and 3) vs reaction coordinate for reactions 1H (solid curves) and 1D (dashed curves). The thin vertical lines denote the locations of the conventional and room temperature variational transition states. Notice that the optimized transition state for reaction 1H at 300 K is at $s^{CVT}_{*H} = 0.110\ a_0$ and the one for reaction 1D is at $s^{CVT}_{*D} = 0.131\ a_0$. (b) Frequencies of the generalized normal modes with e symmetry (modes 4, 5, 6, and 7) vs reaction coordinate for reactions 1H (solid curves) and 1D (dashed curves). The thin vertical lines are the same as in part a.

Table VIII. CVT/SCSAG Per-Site Secondary Deuterium KIEs for $CH_4/CD_3H + H \rightarrow CH_3/CD_3 + H_2$ As Calculated for Three Potential Energy Surfaces[a]

T, K	J1	J2	J3
200	2.04	2.34	1.97
250	1.63	1.86	1.68
300	1.42	1.60	1.50
372	1.27	1.40	1.34
400	1.23	1.35	1.30
500	1.14	1.23	1.20
600	1.10	1.17	1.15
1000	1.04	1.08	1.07
1500	1.03	1.05	1.04

[a] All vibrations harmonic.

are substantial variational effects on individual vibrational contributions which are much larger than the overall variational effect resulting from all the vibrational contributions taken together, which show only a relatively small difference between the conventional TST and CVT calculations.

We hope it will be possible to include the effects discussed here to improve detailed transition state modeling efforts,[62] which have previously been based on conventional transition state theory without tunneling.

As pointed out by Melander and Saunders,[8] "experimentally α-deuterium isotope effects are almost always substantially less than 1.4". Of course the present case is somewhat atypical of the kind of large-molecule solution-phase reaction upon which that generalization is based. Nevertheless it places our predicted KIEs for $T < 300$ K (see the last column of Table III) in a dramatic light, especially since conventional TST falls well within the 1.4 limit. This then provides an exciting challenge to experimentalists to measure the secondary deuterium KIE for the "simplest" sp^3-to-sp^2 transformation at temperatures below room temperature.

Although the major goal of this paper has been to compare conventional and improved dynamical theories to each other for the *same* potential energy surface, this question of eventual comparison to experiment raises the question of sensitivity of the results to the potential energy surface. To provide some information on this we also computed the secondary deuterium KIE for two other potential energy surfaces that have been proposed,[27] namely surfaces J2 and J3. The resulting KIEs, in all cases based on harmonic vibrations, are compared in Table VIII. There is some sensitivity, but the KIEs are qualitatively similar, and they rise above 1.4 for all three potential functions.

3. Multidimensional Effects in Tunneling. In order to explore the nature of the multidimensional tunneling effects, we also compare the SCSAG treatment of tunneling to a simpler one,[17,33,63] called the minimum-energy path or zero-curvature approximations in which the transmission coefficient is calculated in the same way as SCSAG but neglecting reaction-path curvature. The MEPSAG calculation still includes multidimensional zero-point effects as reflected in the vibrationally adiabatic ground-state potential curve,[17,63] but it does not include corner cutting.[13,33,64] The two kinds of transmission coefficient are compared in Table IX, which also shows their contributions η_{tun}^{CVT} to the final kinetic isotope effect η. There are significant differences between η_{tun}^{CVT} based on the MEPSAG method and η_{tun}^{W}, which equals 1.01 over the whole temperature range. There are even larger differences of η_{tun}^{CVT} based on the SCSAG method from either of these. It is especially interesting to compare the MEPSAG results for 200 K to the SCSAG ones for 300 K. This shows that η_{tun}^{CVT} for the two methods is similar if they are compared at respective temperatures where they predict similar tunneling enhancements. But when they are compared at the same temperature, the SCSAG method yields larger transmission coefficients and hence larger values for η_{tun}^{CVT}.

We conclude that the contribution of tunneling cannot be assumed to cancel in the KIE even when the imaginary frequency characterizing the barrier top is essentially unchanged by isotopic substitution. The isotopic dependence of our more accurate calculations of tunneling arises first because of the zero-point energy contributions of transverse modes to the effective barrier for tunneling, and this is greatly amplified by reaction-path-curvature-promoted corner-cutting effects. A large tunneling effect on the α-deuterium secondary KIE does *not* require coupling secondary C–D motions into the imaginary-frequency normal mode of the transition state.

Although most previous work on α-deuterium secondary kinetic isotope effects has attributed negligible effects to tunneling, the papers of Ostović et al.,[44] Huskey and Schowen,[45] and Saunders and Klinman and their co-workers[46,47] provide important exceptions. Ostović et al.[44] proposed a significant tunneling contribution to secondary kinetic isotope effects in reactions involving hydride transfer between NAD^+ analogues; more specifically they interpreted their observed KIEs as due to participation of the nontransferred hydrogen in the reaction coordinate for tunneling. Huskey and Schowen[45] noted that tunneling effects provide a consistent explanation for "anomalous" α-D KIEs which, although smaller than calculated here, exceed the corresponding equilibrium isotope effects. Saunders[46] reported model studies of β-hydrogen secondary kinetic isotope effects in E2 reactions that indicate an important effect of tunneling due to coupling of the stretching mode of a transferred H with a bending mode involving nontransferred H, and in a followup experimental paper Amin et al.[46] tested the predictions of his model. Saunders' work suffers, however, from the deficiencies of the infinite parabolic one-dimensional treatment of tunneling as discussed above. Finally we mention the recent work of Klinman and co-workers. They studied primary and secondary KIEs for both deuterium and tritium for enzyme-catalyzed oxidation reactions. For the oxidation of benzyl alcohol to benzaldehyde, a high tritium secondary KIE was interpreted as evidence for tunneling.

4. Other Reactions

We also considered the reverse reactions of the ones we have been discussing, namely

$$CH_3 + H_2 \rightarrow CH_4 + H \quad \text{(reaction -1H)}$$

$$CD_3 + H_2 \rightarrow CD_3H + H \quad \text{(reaction -1D)}$$

and we considered

$$CH_4 + D \rightarrow CH_3 + HD \quad \text{(reaction 2H)}$$

$$CD_3H + D \rightarrow CD_3 + HD \quad \text{(reaction 2D)}$$

1. Reverse Reactions. Now we consider reactions -1H and -1D. For the reverse reactions all diatomic properties cancel in the KIEs, which depend therefore on the properties of $H_3C–H–H$, $D_3C–H–H$, CH_3, and CD_3. For the reverse reactions symmetry effects cancel, and k_H/k_D and the per-site KIE are the same. Table X gives the secondary deuterium KIEs. All the KIEs for these reactions are inverse ($\eta < 1$). In particular, the calculated inverse KIEs in the absence of tunneling are strong enough to overcome the normal contribution from tunneling; thus the net KIE is inverse, as expected (see Introduction). In fact the calculated inverse effects are more dramatic than for typical organic reactions. For example the room temperature value $\eta^{CVT/G} = 0.7$ deviates from unity by 50% more than the value of ~0.8 which has been estimated[39,40] to be the limiting value for complete $sp^2 \rightarrow sp^3$ conversion at the transition state.

Table XI shows the factorization of the KIEs into contributions from different kinds of motion. Clearly the inverse KIE and its temperature dependence are both dominated by the vibrational motions in this case. Thus it is necessary to understand the vibrational contributions in detail.

For the reverse reaction the modes of $H_3C–H–H$ correlate to those of $CH_3 + H_2$ as follows (see Table I): Mode ν_1 of $H_3C–H–H$ with a_1 symmetry is correlated to the ν_1 symmetric stretch in CH_3 so that the vibrational partition functions for these motions are labeled $Q_{vib,1}^{\ddagger}$, $Q_{vib,1}^{GT}$, or $Q_{vib,1}^{R}$. Mode ν_2 of $H_3C–H–H$ with a_1

(62) See, e.g.: Hogg, J. L.; Rodgers, J.; Kovach, I.; Schowen, R. L. *J. Am. Chem. Soc.* **1980**, *102*, 79. McKenna, J.; Sims, L. B.; Williams, I. H. *J. Am. Chem. Soc.* **1981**, *103*, 268.

(63) Truhlar, D. G.; Kuppermann, A. *J. Am. Chem. Soc.* **1971**, *93*, 1840.

(64) Marcus, R. A. *J. Chem. Phys.* **1966**, *45*, 4493, 1969, 49, 2617. Marcus, R. A.; Coltrin, M. E. *J. Chem. Phys.* **1977**, *67*, 2609.

Table IX. Effect of Neglecting Reaction-Path Curvature on the Multidimensional Semiclassical Transmission Coefficients and Final Calculated KIEs for Reactions 1H and 1D

	CVT/MEPSAG				CVT/SCSAG			
T, K	κ_H	κ_D	η_{tun}^{CVT}	η	κ_H	κ_D	η_{tun}^{CVT}	η
200	5.4	4.6	1.17	1.57	69.2	45.4	1.52	2.04
250	2.7	2.5	1.08	1.37	12.3	9.6	1.28	1.63
300	1.91	1.83	1.05	1.27	5.3	4.5	1.17	1.42
400	1.42	1.39	1.02	1.16	2.4	2.3	1.08	1.23

Table X. Secondary Deuterium KIEs for $CH_3/CD_3 + H_2 \rightarrow CH_4/CD_3H + H$

T, K	η^*	$\eta^{*/W}$	$\eta^{*/lP}$	η^{CVT}	$\eta^{CVT/G}$
200	0.31	0.32	*a*	0.39	0.59
250	0.43	0.43	0.46	0.51	0.65
300	0.53	0.53	0.54	0.60	0.70
372	0.64	0.64	0.65	0.69	0.77
400	0.68	0.68	0.68	0.73	0.79
500	0.77	0.77	0.77	0.80	0.85
600	0.83	0.83	0.83	0.85	0.89
1000	0.94	0.93	0.93	0.94	0.98
1500	0.97	0.97	0.97	0.97	1.00

[a] See footnote *a* in Table II.

Table XI. The Contributions of Various Types of Motion to η^* and η^{CVT} for the Reactions $CH_3/CD_3 + H_2 \rightarrow CH_4/CD_3H + H$

T, K	η_{trans}	η_{rot}^*	η_{vib}^*	η_{rot}^{CVT}	η_{vib}^{CVT}	η_{pot}^{CVT}
200	1.03	1.58	0.19	1.58	0.27	0.86
250	1.03	1.58	0.26	1.58	0.35	0.90
300	1.03	1.58	0.32	1.58	0.40	0.92
372	1.03	1.58	0.39	1.58	0.45	0.94
400	1.03	1.58	0.41	1.58	0.47	0.95
500	1.03	1.58	0.47	1.58	0.51	0.97
600	1.03	1.58	0.51	1.58	0.53	0.98
1000	1.03	1.58	0.57	1.58	0.58	1.00
1500	1.03	1.58	0.60	1.58	0.60	1.00

symmetry is correlated to the H_2 stretch ν_{H_2} so that the vibrational partition function of this mode of reactants is called $Q_{vib,2}^R$ instead of $Q_{vib}^{H_2}$. The transition state umbrella mode ν_3 with a_1 symmetry is correlated to the out-of-plane bending mode ν_2 is CH_3 so the vibrational partition function of this mode of the reactant is referred to as $Q_{vib,3}^R$. The vibrational mode ν_4 of H_3C-H-H with e symmetry is correlated to the doubly degenerate C–H asymmetric stretch, ν_3, in CH_3. Thus the corresponding partition function of this reactant mode is denoted as $Q_{vib,4}^R$. The ν_5 mode of e symmetry is correlated to the in-plane bend, ν_4, in CH_3. The remaining two doubly degenerate frequency motions, ν_6(e) and ν_7(e), of H_3C-H-H do not correlate to bound vibrational motions in the reactant $CH_3 + H_2$.

For the reverse reactions, the three lowest frequency vibrations, m = 3, 6, and 7, of the transition state are responsible for the inverse contribution to the secondary deuterium KIE, as seen in Table XII. The m = 4 motion makes almost no contribution to the secondary KIEs, and the m = 2 mode also makes minor contributions; however, the m = 1 and 5 vibrations both make substantial normal contributions at 300 K. The normal contributions from these modes, however, are outweighed by the inverse contributions from the m = 3, 6, and 7 modes.

As expected several of the modes show opposite-type contributions for the forward and reverse reactions (compare Tables VII and XII). This includes the m = 3 umbrella motion, which is normal for the forward reactions and inverse for the reverse reaction. The same situation occurs for m = 6; and the m = 4 and 5 modes lead to inverse contributions for the forward reaction and normal contributions for the reverse reaction. The ν_7 vibration, which does not correlate to any bound motion of reactants for either the forward or the reverse reactions, has a significant inverse contribution to the secondary deuterium KIEs in both cases since it is more constrained in the perprotio transition state than in the deuterated one. The m = 1 mode gives a normal contribution for the forward reaction at low temperature and becomes slightly inverse as the temperature increases. However, this C–H stretch motion gives a normal contribution for the reverse reaction. A normal contribution from the m = 2 mode is predicted at high temperature for both forward and reverse reactions.

For the reverse reaction at 300 K, there is a 40% difference between $\eta_{vib,1}^*$ and $\eta_{vib,1}^{CVT}$, about 17% difference between $\eta_{vib,5}^*$ and $\eta_{vib,5}^{CVT}$, and about 31% difference between $\eta_{vib,6}^*$ and $\eta_{vib,6}^{CVT}$.

2. $CH_4/CD_3H + D \rightarrow CH_3/CD_3 + HD$. Finally we consider the reaction of methane with a deuterium atom. This has a larger reaction-path curvature than the reactions examined above. As discussed in the Introduction, for reactions with intermediate or large reaction-path curvature, the larger of the SCSAG and LCG3 transmission coefficients is accepted as more reasonable.[34] The transmission coefficients calculated for $CH_4 + D$ and $CD_3H + D$ are given in Table XIII. From these results we conclude that the tunneling contributions to the secondary deuterium KIEs for reactions 2H and 2D should be computed with the LCG3 method, and we will do so.

Again the multidimensional tunneling calculations indicate that the tunneling effect, in particular its isotopic dependence, is poorly described by the Wigner or infinite parabolic one-dimensional treatments. Furthermore tunneling is so important that the secondary KIE may not be understood even qualitatively correctly without consideration of the proper tunneling contributions.

The kinetic isotope effects and Arrhenius parameters for reactions 2H and 2D are listed in Tables XIV and XV, respectively. Again we see large effects of using variational rather than conventional transition states and of including multidimensional tunneling contributions.

From Table XIV, it is clear that the variational effect on the secondary deuterium KIEs, i.e., the difference between η^{CVT} and η^*, is significant. At room temperature or lower, the variational effect is greater than 10%. As for the other reactions studied, the Wigner correction for the tunneling, which was used in the previous theoretical study,[32] gives almost no contribution to the secondary deuterium KIEs, i.e., we obtain almost the same values

Table XII. The Contributions of Various Modes or Degenerate Pairs of Modes to η_{vib}^* and η_{vib}^{CVT} for $CH_3/CD_3 + H_2 \rightarrow CH_4/CD_3H + H$

	$\eta_{vib,1}$		$\eta_{vib,2}$		$\eta_{vib,3}$		$\eta_{vib,4}$		$\eta_{vib,5}$		$\eta_{vib,6}$		$\eta_{vib,7}$	
T, K	*	CVT	*	CVT	*	CVT	*	CVT	*	CVT	*	CVT	*	CVT
200	1.00	1.98	0.98	0.85	0.63	0.64	1.05	1.03	2.86	1.45	0.23	0.38	0.49	0.44
250	0.99	1.63	0.98	0.91	0.70	0.71	1.05	1.03	2.33	1.38	0.29	0.46	0.55	0.50
300	1.00	1.40	0.99	0.97	0.77	0.77	1.03	1.02	2.05	1.35	0.35	0.51	0.59	0.55
372	1.00	1.21	0.99	1.05	0.82	0.83	1.03	1.03	1.80	1.32	0.43	0.56	0.63	0.58
400	1.00	1.15	0.99	1.07	0.85	0.86	1.01	1.01	1.73	1.31	0.45	0.57	0.63	0.60
500	1.00	1.04	0.99	1.11	0.87	0.88	1.02	1.01	1.58	1.31	0.51	0.60	0.65	0.63
600	1.00	1.02	0.99	1.10	0.91	0.90	1.02	1.01	1.51	1.30	0.55	0.62	0.67	0.65
1000	1.00	1.01	0.99	1.04	0.96	0.96	1.01	1.01	1.38	1.32	0.62	0.64	0.69	0.68
1500	1.01	1.01	1.00	1.02	0.97	0.98	1.00	1.00	1.34	1.33	0.65	0.65	0.70	0.70

Table XIII. Transmission Coefficients for Reactions 2H and 2D as Functions of T

reactant	κ	200 K	250 K	300 K	400 K	500 K	600 K
CH_4	W	3.11	2.35	1.94	1.53	1.34	1.23
	IP	*a*	9.74	3.40	1.82	1.44	1.28
	SCSAG	28.0	8.22	4.29	2.27	1.69	1.44
	LCG3	93.7	21.5	9.09	3.60	2.28	1.77
CD_3H	W	3.08	2.33	1.92	1.52	1.33	1.23
	IP	*a*	9.01	3.31	1.80	1.43	1.27
	SCSAG	17.2	5.87	3.36	1.96	1.54	1.35
	LCG3	36.0	10.5	5.14	2.48	1.77	1.48

[a] The infinite parabolic formula is again not applicable at 200 K.

Table XIV. Secondary Deuterium KIEs for $CH_4/CD_3H + D \rightarrow CH_3/CD_3 + HD$

T, K	$\eta^{\ddagger}$	$\eta^{\ddagger/W}$	$\eta^{\ddagger/IP}$	η^{CVT}	$\eta^{CVT/LCG3}$
200	1.07	1.08	*a*	1.31	3.09
250	1.08	1.08	1.16	1.25	2.51
300	1.07	1.08	1.10	1.19	2.07
400	1.05	1.05	1.06	1.09	1.60
500	1.03	1.03	1.04	1.04	1.38
600	1.02	1.02	1.02	1.01	1.28
1000	1.00	1.00	1.00	0.99	1.12

[a] The infinite parabolic formula is again not applicable at 200 K.

Table XV. Kinetic Isotope Effects on Arrhenius Parameters for Reactions 2H and 2D at 300–372 K

	A_H/A_D	$E_{a,D} - E_{a,H}$, kcal/mol
‡	0.99	0.04
‡/W	0.99	0.05
‡/IP	0.95	0.09
CVT	0.86	0.19
CVT/G	0.73	0.62

for $\eta^{\ddagger}$ and $\eta^{\ddagger/W}$. Similarly $\eta^{\ddagger/IP}$ agrees with $\eta^{\ddagger}$ within 7%. However, the multidimensional LCG3 tunneling calculations indicate that the tunneling contribution is very important in this case, with a difference between η^{CVT} and $\eta^{CVT/LCG3}$ of more than 80%.

5. Conclusion

The secondary deuterium KIEs for hydrogen-transfer reactions are almost always interpreted in terms of conventional transition state theory. The present article shows that variational transition state theory calculations with multidimensional semiclassical ground-state transmission coefficients lead to significantly different secondary deuterium KIEs as compared to conventional TST. Small structural differences between conventional and variational transition states have significant effects on the nontunneling KIEs, and the final KIEs are affected significantly by multidimensional tunneling contributions that are much more sensitive to α-deuterium substitution than previous theoretical treatments would suggest. Experimental tests of these predictions would be most welcome. In their absence, however, since the present model has proved more reliable than conventional TST when tests are possible,[10-14] we urge great caution in interpreting secondary deuterium KIEs by conventional transition state theory.

Detailed analysis of the factors entering the calculated KIEs provides insight into the physical origins of the effects. The secondary deuterium KIEs for reactions such as those studied here, for which the central carbon atom of the system changes from tetrahedral sp^3 hybridization to planar sp^2 hybridization, favor the undeuterated species in the forward reaction and the deuterated species for the reverse conversion. These tendencies are found to be more pronounced for the forward reactions and less pronounced for the reverse reaction than predicted by conventional transition state, both because of variational effects on the location of the best dynamical bottleneck and also because of important tunneling effects found in this study, which always increase k_H/k_D for these reactions. Previous interpretations of experimental work have ignored variational effects and significantly underestimated the tunneling effect, which will lead to incorrect interpretations of vibrational contributions. In particular when secondary KIEs are studied in the usual inverse mode, i.e., the potential surface or structure of the activated complex is inferred from the KIE (whereas here we calculate the KIE from the structure and potential surface), the use of conventional transition state theory for either the forward or reverse reaction would lead to inferred saddle point structures that are too far toward the sp^2 limit in order to compensate for the neglect of these effects. Therefore, the previous interpretations must be re-evaluated carefully.

We have made a detailed analysis of the contributions of the individual vibrational degrees of freedom to the secondary deuterium KIE. The major inverse contributions for the $CH_4 + H$ reaction come from three transition state vibrations: vibrational mode ν_4, which evolves from an asymmetric CH stretch, ν_5, which correlates to the H–C–H bend, and ν_7, which does not correlate to any bound motion in reactants. For the reverse reaction $CH_3 + H_2$, the major inverse contributions result from the three motions with lowest vibrational frequencies at the transition state: ν_3, the umbrella motion corresponding asymptotically to the out-of-plane bend of the methyl group, ν_6, the doubly degenerate H–C–H bending mode, and ν_7, which correlates with a free motion of the two reactants. Significant variational effects on the contributions from several vibrational degrees of freedom are very important for quantitative understanding of the secondary deuterium KIEs.

Acknowledgment. We are grateful to W. H. Saunders for comments on the original manuscript. D.M. is grateful for a Lando-SOHIO Summer Undergraduate Research Fellowship. This work was supported in part by the U.S. Department of Energy, Office of Basic Energy Sciences, and by Minnesota Supercomputer Institute.